Chlorophenol Dehalogenation in a Magnetically Stabilized Fluidized Bed Reactor

Lisa J. Graham, James E. Atwater and Goran N. Jovanovic
Dept. of Chemical Engineering, Oregon State University, 103 Gleeson Hall, Corvallis, OR 97331

DOI 10.1002/aic.10681
Published online October 20, 2005 in Wiley InterScience (www.interscience.wiley.com).

Aromatic halocarbons are often present in contaminated aquifers, surface waters, wastewater streams, soils, and hazardous wastes. The dehalogenation of p-chlorophenol as a model compound in both the aqueous phase and in slurries of contaminated solids using a magnetically stabilized fluidized bed (MSFB) reactor is discussed. Composite palladium-iron (Pd/Fe) media are employed as both catalyst and sacrificial reactant for the reductive dechlorination of p-chlorophenol. Calcium alginate beads impregnated with Pd/Fe granules are fluidized in a recirculating aqueous stream containing either dissolved p-chlorophenol or a slurry of soil contaminated with this chlorocarbon. Magnetic stabilization of the fluidized bed allows substantially higher rates of mass transfer than would otherwise be achievable, and allows circulation of contaminated solids while fluidization media are retained. Anoxic conditions are sustained under a nitrogen purge and the solution pH of 5.8 is maintained by active control to minimize surface fouling by hydroxides, and to minimize mass-transfer resistances resulting from the surface accumulation of hydrogen bubbles. A model of this process is described and the resulting predictions are compared to the experimentally derived data. © 2005 American Institute of Chemical Engineers *AIChE J,* 52: 1083–1093, 2006
Keywords: decolorination, magnetic field, paladium catalyst, sludge, fluidized bed, fluidization, catalysis, environmental engineering, reaction kinetics, suspensions

Introduction

Chlorophenols are ubiquitous, toxic, and persistent environmental contaminants, many of which are classified as priority pollutants by the U.S. Environmental Protection Agency (EPA). Primary uses include the synthesis of dyes, plant growth regulators, and herbicides. Chlorophenols, which are relatively resistant to natural biodegradation processes, occur in a variety of industrial effluents, polluted soils, sludges, and groundwaters. Chlorophenols are also produced during paper pulp bleaching and drinking water disinfection. Degradation of this important class of problematic environmental contaminant has been studied extensively by a wide variety of methods, including: ozonation,[1-3] Fenton peroxidation,[4,5] peroxidation via heterogeneous catalysis,[6-8] photoperoxidation,[9] photo-Fenton peroxidation,[10-12] electrochemical oxidation,[13-15] electrochemical reduction,[16,17] photoelectrochemical oxidation,[18] catalytic hydrodechlorination,[19,20] reduction with zero valent metals,[21,22] and oxidation in supercritical water.[23-25] Numerous photocatalytic studies of chlorophenol degradation have also been reported using titania,[26-28] cadmium sulfide,[29] and polyoxometalates.[30]

Here we report the reductive dehalogenation of *p*-chlorophenol using bimetallic palladium - iron (Pd/Fe) media in a magnetically stabilized fluidized-bed (MSFB) reactor to produce phenol and hydrogen chloride. The main motivation for this work stems from numerous challenges in the cleanup of "*legacy mixed waste*". This type of waste contains, among other contaminants, poly-chlorinated byphenyls often mixed with a sludge type material. The dehalogenation process presented in this work should be viewed as a development of a model

Correspondence concerning this article should be addressed to G. N. Jonanovic at goran@engr.orst.edu.

reaction process using a model compound (*p*-chlorophenol) in both the aqueous phase and in a slurry of contaminated solids.

p-chlorophenol is moderately soluble in water, with reported values ranging between 20.8 – 23.2 g/L at temperatures between 15 and 25 °C.[31,32] The employment of palladium as a catalyst to promote liquid phase hydrodehalogenation reactions has been studied extensively for chlorocarbons in general,[33-35] and for chlorophenols in particular.[19,20] The benefits of employment of this catalyst in conjunction with metallic iron as a sacrificial reductant have been reported by Wang and Zhang,[36] Lien and Zhang,[37] Kim and Carraway,[38] Liu et al.,[39,40] Guasp and Wei,[41] and Zhou et al.[42] The application of Pd/Fe media in the reduction of *p*-chlorophenol has been studied in preliminary work reported by Graham and Jovanovic.[43]

Magnetically stabilized fluidized bed (MSFB)

The MSFB consists of an axial magnetic field applied to a traditional fluidized bed containing ferromagnetic or ferrimagnetic media.[44-50] Within the MSFB, magnetically susceptible fluidization media are magnetized, resulting in additional attractive and repulsive interparticle forces. Individual particles within the magnetized fluidized bed behave as magnetic dipoles and associate with one another to form clusters and chains which are bound together by magnetic force. Collectively, these magnetically bound groupings present greater mass, as compared to individual particles, and thereby exhibit increased gravitational resistance to drag forces. Thus, the interstitial fluid velocity can be increased to achieve an equivalent degree of fluidization relative to a conventional fluidized bed. This phenomenon allows substantial improvements in rates of mass transfer between the fluid and magnetically susceptible solids, while aiding retention of the media within the bed.[51-54] Additional direct body forces may be produced on ferromagnetic fluidization media by magnetic field gradients as shown in Eq. 1.[55]

$$\mathbf{F_m} = \nabla(\mathbf{M} \cdot \mathbf{B}) \tag{1}$$

Here the force vector, equivalent to the gradient of the inner product of magnetization and flux density, is collinear with the magnetic field gradient. If the gradients are directed toward the distributor, an additional magnetic stabilization force results. Enhanced mass transfer and conversion rates, similar to those obtained in packed beds, are routinely obtained while the highly desirable characteristics of fluidized beds (that is, low-pressure drop and the ability to process solids) are retained. The employment of MSFB methods in liquid-solid systems has been studied by several investigators.[56-59] Aqueous phase applications include affinity separations[60-62] and bioreactor operations.[63,64]

Pd/Fe dechlorination reaction chemistry

As discussed by Graham and Jovanovic,[43,65] three separate components contribute to the overall dechlorination reaction. These include *surface reactions, solution reactions,* and the *chlorine removal* reaction. The surface reactions include the dissolution of iron from the zero-valent state and hydrogen ion consumption on both the iron and palladium surfaces as represented by Eqs. 2, 3 and 4, respectively

$$Fe^0 \rightarrow Fe^{2+} + 2e^- \tag{2}$$

$$2H^+ + 2e^- \xrightarrow{Fe} H_2(g) \tag{3}$$

$$H^+ + e^- \xrightarrow{Pd} H^* \tag{4}$$

The abundance of hydrogen ion is controlled by its formation from the dissociation of water and the ionization of hydrogen chloride as shown in Eqs. 5 and 6

$$2H_2O \rightarrow 2H^+ + 2OH^- \tag{5}$$

$$2HCl \rightarrow 2H^+ + 2Cl^- \tag{6}$$

and its removal by Fe or Pd to form the intermediate reactive hydrogen, H*.[66,67] The electrons produced in the iron dissolution reaction are utilized by the palladium surface to form the highly reactive intermediate *H**, which is used in the dechlorination reaction

$$2H^* + R\text{—}Cl \rightarrow R\text{—}H + HCl \tag{7}$$

Coupling the steps together from equations 2, 4, and 7 gives the overall reaction shown in Eq. 8.

$$Fe^0 + R\text{—}Cl + H^+ \rightarrow R\text{—}H + Fe^{2+} + Cl^- \tag{8}$$

Additional parameters which affect the kinetics of this overall reaction include pH and dissolved O_2, which are responsible for $Fe(OH)_2$ and $Fe(OH)_3$ formation, and for the oxidation of Fe(II) to Fe(III), respectively.

System Modeling

Chemical reaction kinetics

As a heterogeneous reaction, the disappearance of the chlorinated solute *A*, depends on the concentrations of *A* and *H**, and also upon the quantity of Fe/Pd reductant-catalyst *W*, as in Eq. 9

$$-\frac{1}{W}\frac{d(VC_A)}{dt} = k'C_AC_{H^*} \tag{9}$$

Assuming a constant pH and, therefore, a constant rate of H* formation from H^+ at the palladium catalyst surface, a pseudo first-order rate expression results, which when H* and *W* are incorporated into the rate constant, yields Eq. 10.

$$-\frac{d(VC_A)}{dt} = (Wk'C_B)C_A = (Wk)C_A = k^*C_A \tag{10}$$

To account for the effects of passivation or deactivation on the Pd/Fe surface, an activity term *a*, is integrated into the reaction kinetics as shown in Eq. 11.

$$-\frac{d(VC_A)}{dt} = (kW)C_A a = k^* C_A a \tag{11}$$

This expression accounts for the decrease in active surface area of the solid phase which corresponds to a loss of both available catalyst and reductant, as well as deactivation mechanisms, such as catalyst passivation due to H_2(g) bubble or hydroxide formation. The activity of the catalyst is further described by Eq. 12 for an n^{th} order deactivation process.

$$-\frac{da}{dt} = k_d a^n \tag{12}$$

Diffusion and reaction in alginate beads with entrapped Pd/Fe

The following assumptions were employed in the derivation of the diffusion model: (1) the alginate gel beads are of equal size and are uniform spheres of radius r; (2) a constant effective diffusion coefficient D_e exists throughout the beads, hence, the tortuosity effect on the aqueous diffusion coefficient does not change from the surface of the alginate bead to the center (this assumption implies that alginate beads are homogeneously polymerized and crosslinked); (3) no reaction occurs in the completely mixed bulk liquid as the Pd/Fe is entrapped within the gel beads and not permitted into the bulk liquid; (4) the Pd/Fe particles are homogeneously entrapped within the alginate bead, thus, ensuring a uniform reaction surface throughout the bead; (5) the liquid phase residing within the pore spaces of the bead is defined as a volume fraction of the total bead volume (the symbol, ϕ, represents the fraction of bead occupied by gel and/or entrapped substance); and (6) the "open flux area for diffusion" within the bead is defined as a fraction of the total surface area, and is dependent on the fraction of bead surface occupied by the alginate gel.

A mass balance on the liquid phase within the alginate bead, including both reaction and deactivation mechanisms is given by Eq. 13

$$\frac{\partial C_l(r,\,t)}{\partial t} = D_e\left(\frac{\partial^2 C_l(r,\,t)}{\partial r^2} + \frac{2}{r}\frac{\partial C_l(r,\,t)}{\partial r}\right) - \frac{k^*}{V} C_l(r,\,t)a^n \tag{13}$$

However, if the fluid-particle mass-transfer resistance cannot be neglected as a controlling factor, then the boundary condition at $r = R$ for the alginate bead becomes

$$D_e \frac{\partial C_l(R,\,t)}{\partial r} = k_l\left[C_b(t) - \frac{C_l(R,\,t)}{K_b}\right] \tag{14}$$

A mass balance on the bulk liquid concentration $C_b(t)$ is related to the diffusion at the outer boundary and is given by

$$\varepsilon V \frac{dC_b(t)}{dt} = -Vk_l a\left[C_b(t) - \frac{C_l(R,\,t)}{K_b}\right] \tag{15}$$

The initial conditions for the bulk and bead liquid and the boundary condition for the center of the bead, are given by Eqs. 16–18, respectively

$$C_l(r,\,t=0) = C_{l,0} \tag{16}$$

$$C_b\,(t=0) = C_{b,0} \tag{17}$$

$$\left.\frac{\partial C_l(r,\,t)}{\partial r}\right|_{r=0} = 0 \tag{18}$$

Modeling of p-chlorophenol dechlorination in contaminated soil using alginate entrapped Pd/Fe

To model the desorption and subsequent reaction of *p*-chlorophenol, it is important to characterize the soil surface. To quantify the abundance of adsorbed organic material on the soil at equilibrium, a sorption isotherm for *p*-chlorophenol on Willamette type soil is developed. Important parameters of the soil include the fraction of organic matter, the fraction of organic carbon, and the tendency of the contaminant to adsorb onto the soil which is expressed as the solid-water distribution ratio $K_{d,s.}$ A common experimental method of determining the solid-water distribution ratio involves the application of a Freundlich isotherm, where p measures nonlinearity

$$C_s = K_{d,s} * C_b^p \tag{19}$$

The distribution ratio $K_{d,s,}$ was experimentally determined from sorption isotherm for *p*-chlorophenol on Willamette type soil at 20 °C and pH = 6.0 ± 0.05. For the concentration range of interest it was found[51] that $K_{d,s} = 1.12$ and $p = 1$. This experimentally obtained value could be compared with the distribution ratio obtained from the correlation reported in literature.[68] Both values are presented in Table 3. Details related to the experimental determination of $K_{d,s}$, as well as the estimate obtained from published correlation are presented by Graham.[51] The equilibrium relationship (Eq. 19) is used when developing the model describing transport of *p*-chlorophenol from the soil to the surrounding bulk liquid.

Another important aspect of dechlorination of *p*-chlorophenol from contaminated soil involves the mechanism of transport to the bulk liquid. To determine a reasonable model, the soil particles were examined by scanning electron microscopy (SEM) to determine their surface properties, as shown in Figure 1(a–d). Based on the analysis of these photomicrographs, it was concluded that the soil particles exhibit an extremely low porosity, which limits the ability of *p*-chlorophenol to diffuse into the interior. The soil particles were also determined to have a bulk density of 2300 ± 60 kg/m^3. Due to the low porosity, the pore diffusion of the contaminant is considered negligible for modeling purposes, and only mass transfer from the surface of the soil particles is considered. The mass balance on the soil particles is given as

$$\frac{dC_s(t)}{dt} = -k_{l,s}a'\left[\frac{C_s(t)}{K_{d,s}} - C_b(t)\right] \tag{20}$$

with the initial condition

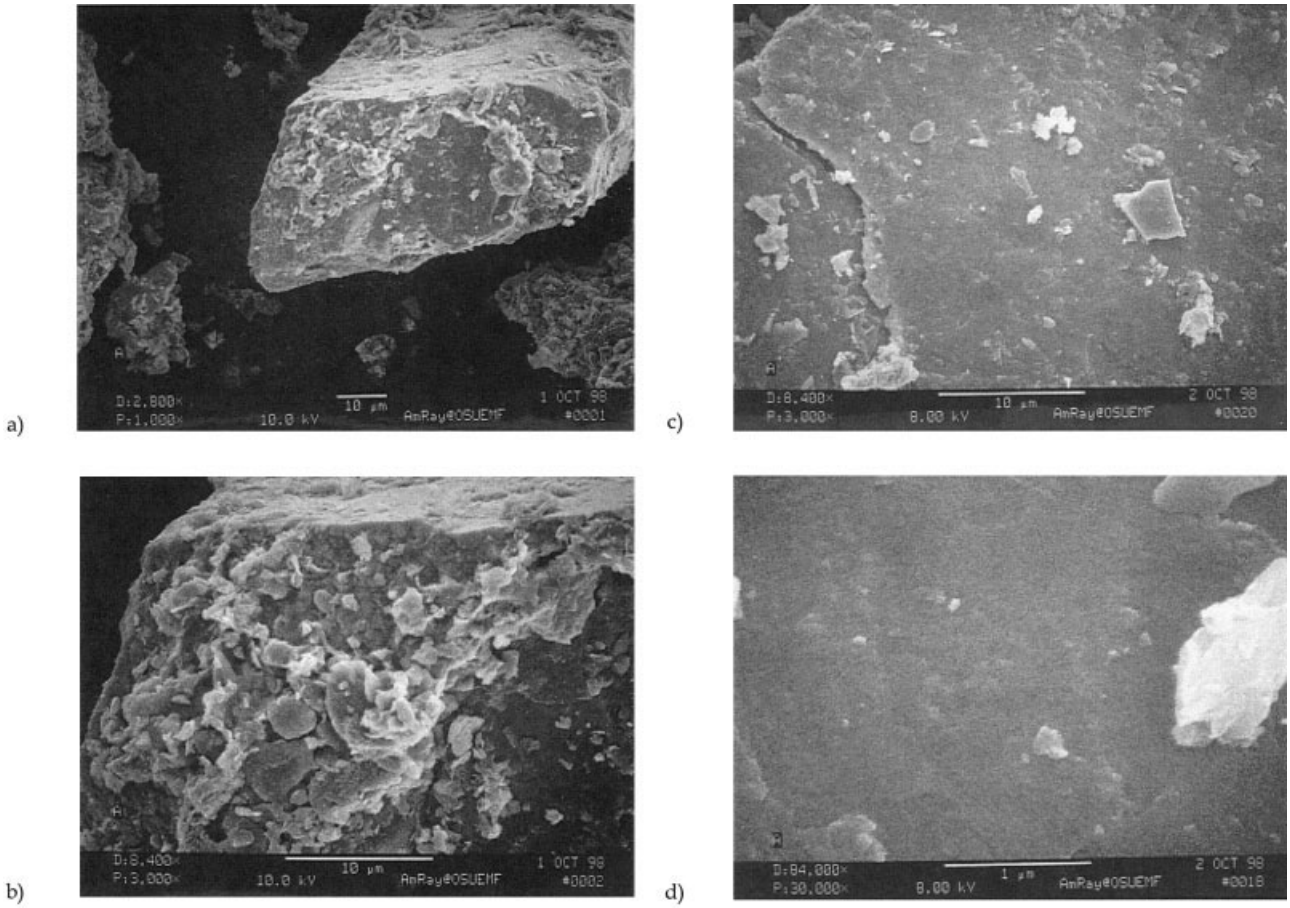

Figure 1. SEM photomicrographs of Willamette Valley soil (54-104 μm), (a) 1000x soil particle, (b) 3000x rough surface, (c) 3,000 x smooth surface, and (d) 30,000 x showing negligible porosity.

$$C_s(t) = C_{s,0}(t) \tag{21}$$

The resulting balance equation for the bulk liquid phase is

$$\varepsilon V \frac{dC_b(t)}{dt} = -Vk_l a[C_b(t) - C_l(R, t)] + k_{l,s}a'\left[\frac{C_s(t)}{K_{d,s}} - C_b(t)\right] \tag{22}$$

with the initial condition for the bulk liquid given by

$$C_b\,(t = 0) = C_{b,0} \tag{23}$$

The mass balance on the liquid within the alginate bead is

$$\frac{\partial C_l(r, t)}{\partial t} = D_e\left(\frac{\partial^2 C_l(r, t)}{\partial r^2} + \frac{2}{r}\frac{\partial C_l(r, t)}{\partial r}\right) - \frac{k^*}{V} C_l(r, t)a^n \tag{24}$$

with the initial condition

$$C_l\,(r, t = 0) = C_{l,0} \tag{25}$$

and boundary conditions

$$D_e \left.\frac{\partial C_l(R, t)}{\partial r}\right|_{r=R} = k_l\left[C_b(t) - \frac{C_l(R, t)}{K_b}\right] \tag{26}$$

and

$$\left.\frac{\partial C_l(r, t)}{\partial r}\right|_{r=0} = 0 \tag{27}$$

Experimental

Pd/Fe fluidization media

Palladized iron was prepared by the spontaneous oxidation-reduction reaction between metallic iron, and the divalent aqueous hexachloropalladate anion. Powdered iron (5–8 μm) was pretreated with 6M HCl for 15 min to remove surface oxides, rinsed twice with deionized water, immersed in an aqueous K_2PdCl_6 solution, and vigorously mixed for 4 min. Completion of the reaction was indicated by a color change from dark orange to pale yellow. The aqueous phase was then decanted and the palladized iron was subsequently rinsed with deionized water and dried. Scanning electron photomicrographs of acid treated Fe(0) and palladized iron bearing distinct nanoscale Pd islets are shown in Figure 2. Pd/Fe media were prepared covering the composition range between 0.02 –

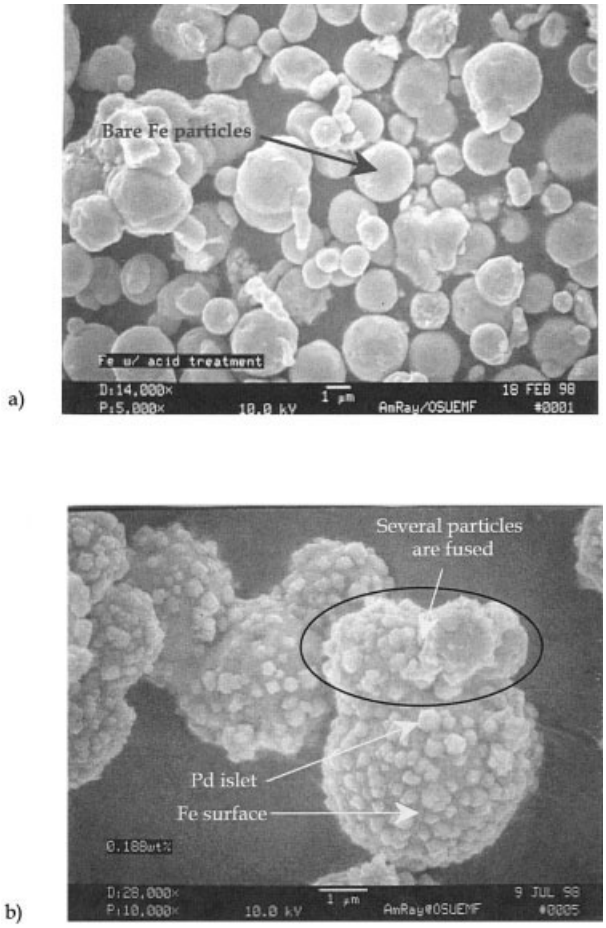

Figure 2. Scanning electron photomicrographs, (a) acid pretreated Fe particles, and (b) Palladized Fe particles.

0.75% Pd (w/w). The results of preliminary experiments indicated that 0.188% (w/w) palladium provided good catalytic activity without restricting access of the reactants to the zero valent iron surface.[43] Hence, this concentration was used in subsequent experiments.

Pd/Fe impregnated calcium alginate beads were then produced. A suspension of the Pd/Fe media was first prepared by addition to a well mixed 1.5% aqueous solution of sodium alginate. The suspension was then extruded through a pressurized narrow bore nozzle by gravity flow, augmented by air flow through the nozzle, into a 1.5 M aqueous calcium chloride crosslinking solution. As the slurry is extruded through the needle, a drop forms on the tip which then falls into the $CaCl_2$

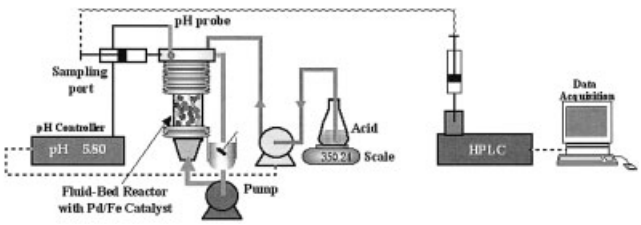

Figure 3. Representation of the magnetically stabilized fluidized bed (MSFB) apparatus.

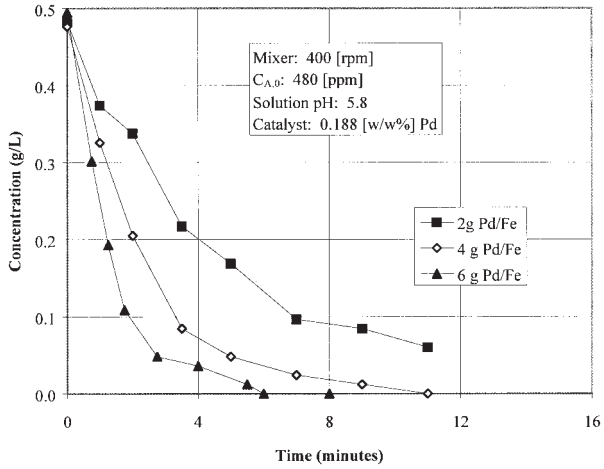

Figure 4. Results of *p*-chlorophenol dechlorination kinetics experiments.

solution, and gels to form a spherical bead. Beads were allowed to gel in the crosslinking solution for 30 min. Bead size is controlled by viscosity and surface tension of the alginate solution, and by the pressure and airflow rate of the particle generator. For this study, beads with nominal diameters of 2 mm and Pd/Fe loadings of 12.0% (w/w), corresponding to a bulk density of 1173 kg/m^3, were employed. The minimum fluidization velocity for these particles under aqueous flow in the absence of an applied magnetic field and magnetic field gradient is 1.04 cm/s.

Chemical kinetic apparatus and method

A stirred-batch reactor was assembled for the characterization of *p*-chlorophenol dehalogenation kinetics, Pd/Fe media

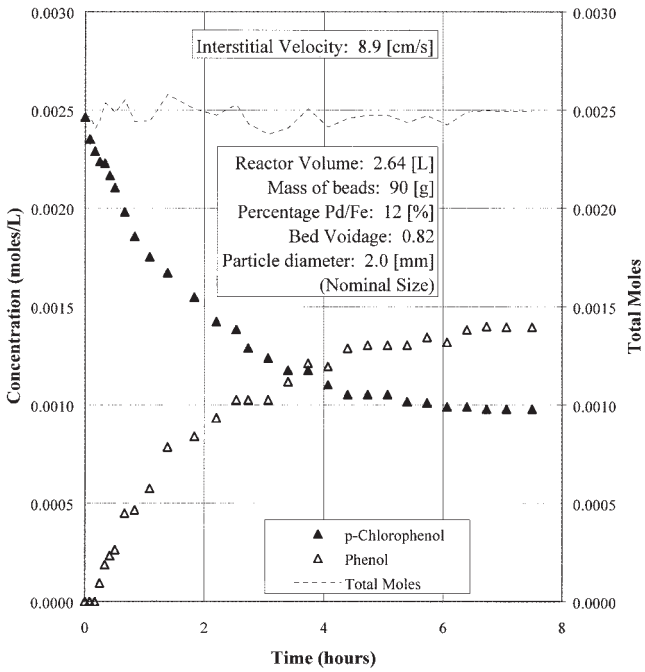

Figure 5. Dechlorination of aqueous *p*-chlorophenol in MSFB without applied magnetic field.

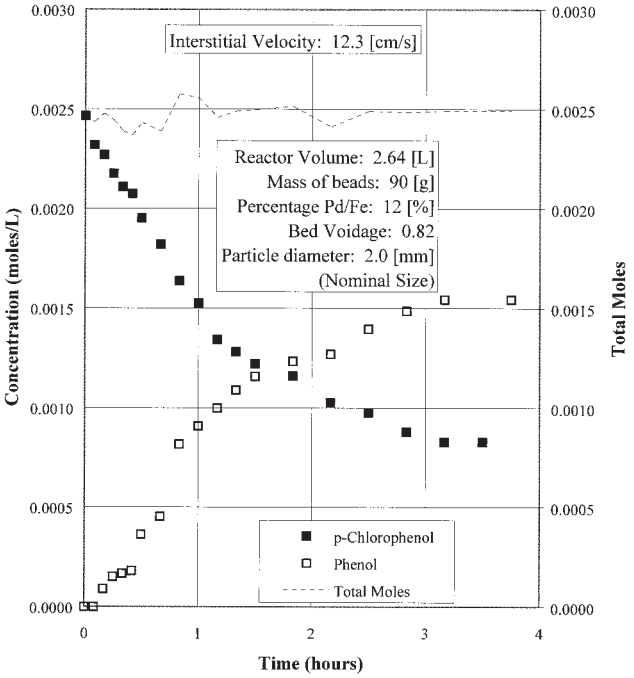

Figure 6. Dechlorination of aqueous *p*-chlorophenol in MSFB with applied magnetic field.

deactivation rates, and the effects of pH and other reaction parameters. The system consists of a 400 mL reactor vessel fitted with a variable speed mixer, pH probe, pH controller, metering pump, acid reservoir containing HCl, sampling port, and a nitrogen purge to maintain anoxic conditions. Using this system, freely suspended Pd/Fe media were continuously and vigorously stirred at a rate sufficient to eliminate mass transfer resistance between the bulk fluid and the palladized iron particles. A known concentration of *p*-chlorophenol was then added to the system, and the changing concentration monitored over time.

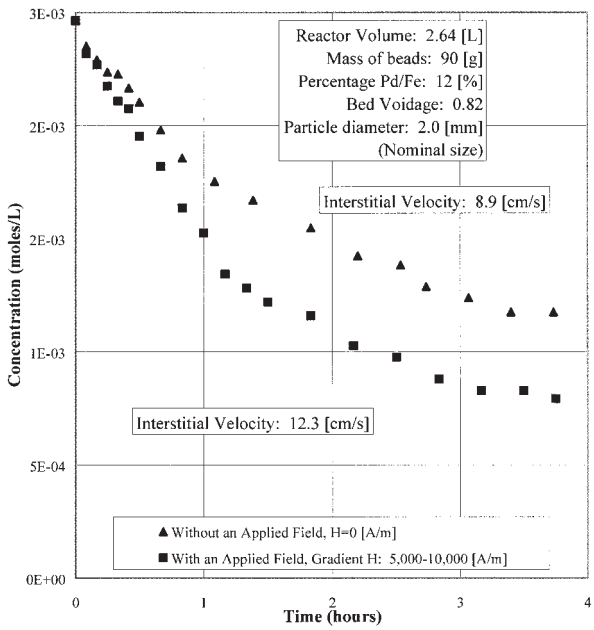

Figure 7. Aqueous phase dechlorinations with and without magnetic field.

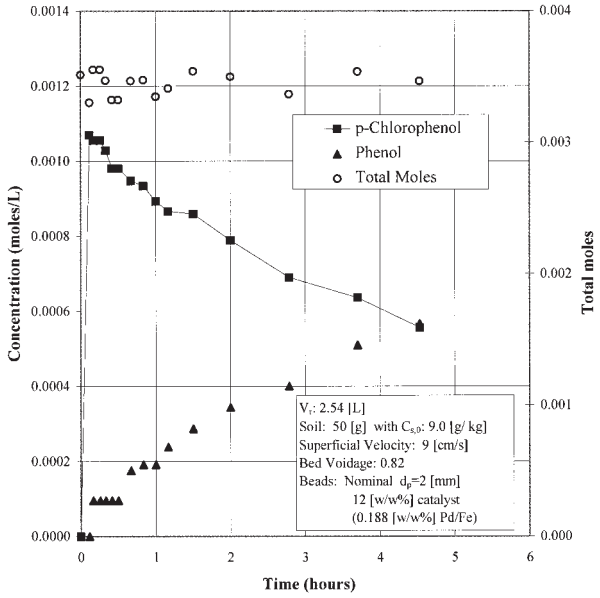

Figure 8. Dechlorination of *p*-chlorophenol contaminated soils in MSFB.

Magnetically stabilized fluidized bed (MSFB) apparatus and experiments

The experimental MSFB apparatus is illustrated in Figure 3. A transparent plastic fluidization column, 45 cm in height with

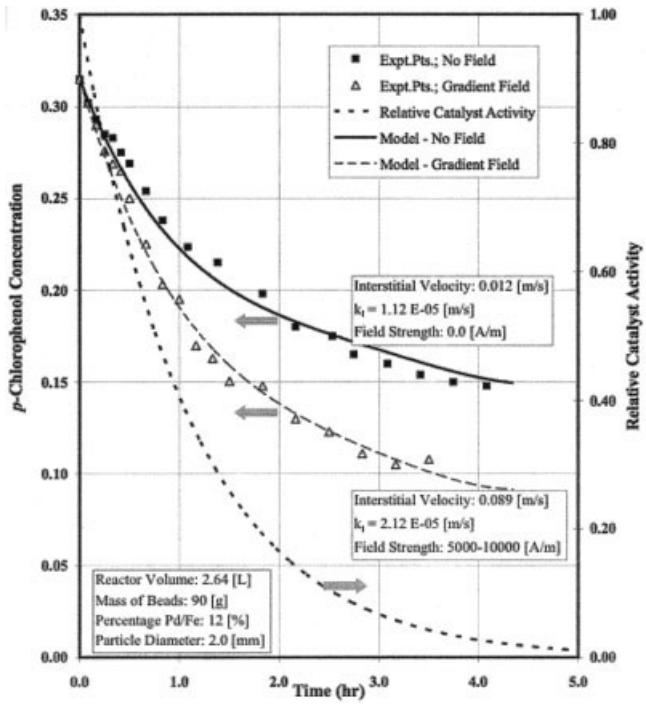

Figure 9. Model predictions and experimental results for MSFB dechlorination of aqueous *p*-chlorophenol.

Table 1. Model Derived Parameters for MSFB Dechlorination of Aqueous *p*-Chlorophenol without an Applied Magnetic Field

Parameter	Units	Optimized Values	Independently Determined Values
k_d	1/s	3.6×10^{-4}	3.62×10^{-4} 1.75×10^{-5} (Fan *et al.,* 1960)[72]
k_l	m/s	1.12×10^{-5}	6.49×10^{-5} (Coderc *et al*., 1972)[73] 3.73×10^{-5} (Cussler, 1984)[74]
k	m^3/s-$kg_{catalyst}$	0.0260	0.0262 8.0×10^{-10} Experiment
D_e	m^2/s	8.2×10^{-10}	7.0×10^{-10} Correlation (Schwarzenbach *et al.*, 1993)[68] 9.3×10^{-10} Correlation (Schwarzenbach *et al*., 1993)[68] 1.1×10^{-9} Correlation (Schwarzenbach *et al*., 1993)[68]

an internal diameter of 3.8 cm, is surrounded by an electromagnet composed of coiled 1 mm dia. copper wire which is energized by a DC power supply. This configuration produces axial magnetic flux densities, and magnetic field strengths ranging between 0.006 – 0.012 T, and 5,000 – 10,000 A/m, respectively. The resulting magnetic field gradients provide an additional downward magnetic body force ($\boldsymbol{F_m}$), as shown in Eq. 1, which operates in conjunction with gravity to oppose drag. Ferromagnetic media within the column are fluidized by a recirculating contaminant laden stream under the action of a peristaltic pump. A sampling port is located at the top of the fluidization column. Here, pH of the recirculating stream is monitored and controlled to maintain pH 5.80 by acid injection (HCl) during experimental runs. All liquid is deoxygenated prior to use and a continuous flow of nitrogen purge gas maintains anaerobic conditions during the experiments. Reductive *p*-chlorophenol dehalogenation experiments were conducted, using both *p*-chlorophenol contaminated aqueous streams and slurries of contaminated soils. Slurries ranging in solids concentrations between 2 – 30% were used.

Analytical method

Phenol and *p*-chlorophenol concentrations were monitored by isocratic reverse phase high-performance liquid chromatography using a methanol-water-acetic acid mobile phase, a C-8 bonded phase silica column, and UV detection at 254 nm.

Results and Discussion

Reaction and deactivation rate constants

The results of previously reported work[43] indicated that acidic and anoxic conditions were required to prevent fouling of the palladized iron surface by hydroxides. Also at low pH, the formation and accumulation of hydrogen bubbles at the solid surface was identified as a source of significant mass-transfer resistance. A pH value of 5.8 was found to provide a reasonable trade-off between these two competing factors. A palladium concentration within the composite Pd-Fe media of 0.188% (w/w) was also found to afford an effective compromise between high catalytic activity of the noble metal and plentiful surface access to the zero valent iron reductant. Therefore, all subsequent reactions were conducted under these conditions. Experimental results using initial Pd/Fe charges of 2, 4, and 6 g in the stirred-tank reactor are shown in Figure 4. Rate constants for the dechlorination reaction and Pd/Fe media deactivation were then derived as first-order processes using the Runge-Kutta-Verner fifth-order and sixth-order method to solve the ordinary differential equations given in Eq. 11 and Eq. 12. This produced values for k and k_d of 0.262 m^3/s-kg and 2.62×10^{-4} s^{-1}, respectively.

MSFB dechlorination of p*-chlorophenol*

Aqueous phase dechlorinations were conducted in the MSFB reactor using 90 g of Pd/Fe impregnated calcium alginate beads and an initial 2.5 mM *p*-chlorophenol concentration. In the first experiment, the media were fluidized in the absence of a magnetic field. The interstitial velocity of 8.9 cm/s produced a bed voidage of 0.83. The resulting decrease in *p*-chlorophenol concentration over time, and the corresponding increase in phenol concentration are illustrated in Figure 5. This was followed by a similar experiment with the solenoid energized to produce the stabilizing magnetic field with axial intensities varying between 5,000 – 10,000 A/m. In this case, an equivalent degree of bed expansion was produced with the substantially increased flow velocity of 12.3 cm/s. Reactant and product concentrations over time are shown in Figure 6. Kinetic curves for the two experiments are compared in Figure 7. Clearly, the global rate of *p*-chorophenol dechlorination under the magnetic field is higher than that for the nonmagnetized condition. This is attributable to the higher degree of reactant mass transfer which can be attained through magnetic stabilization of the fluidization media.

Table 2. Model Derived Parameters for MSFB Dechlorination of Aqueous *p*-Chlorophenol with an Applied Magnetic Field

Parameter	Units	Optimized Values	Independently Determined Values
k_d	1/s	3.6×10^{-4}	3.62×10^{-4} 2.03×10^{-5} (Fan *et al.,* 1960)[72]
k_l	m/s	2.12×10^{-5}	8.98×10^{-5} (Coderc *et al*., 1972)[73] 4.37×10^{-5} (Cussler, 1984)[74]
k	m^3/s-$kg_{catalyst}$	0.0263	0.0262 8.0×10^{-10} Experiment
D_e	m^2/s	8.1×10^{-10}	7.0×10^{-10} Correlation (Schwarzenbach *et al.*, 1993)[68] 9.3×10^{-10} Correlation (Schwarzenbach *et al*., 1993)[68] 1.1×10^{-9} Correlation (Schwarzenbach *et al*., 1993)[68]

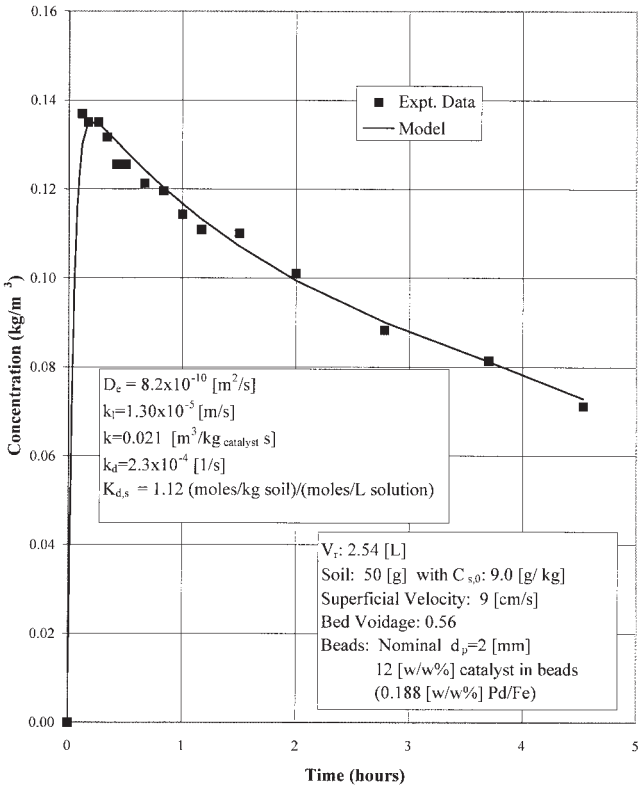

Figure 10. Model predictions and experimental results for MSFB dechlorination of soil contaminated with *p*-chlorophenol.

Similar experiments were subsequently conducted to study the dechlorination of *p*-chlorophenol contaminated soil. Soil collected from the Willamette Valley in western Oregon was employed in this work. Analysis of three soil samples indicated an average organic content of 2.18% (w/w). A 200 g quantity of Pd/Fe-alginate media was charged into the MSFB reactor, and the flow rate was adjusted to produce a superficial velocity of 9.0 cm/s. The recirculating solution was adjusted to pH 5.4 and 50 g of soil contaminated with *p*-chlorophenol at a concentration of 9.0 g per kg of soil was added to the vessel. The soil-water slurry recirculated through the bed, while the ferromagnetic Pd/Fe media were retained within the MSFB. As before, *p*-chlorophenol and phenol concentrations were monitored in the aqueous phase over time. Experimental results are summarized in Figure 8. Here the initial concentrations of both analytes are zero, since before dechlorination reactions can commence, the bound halocarbon must first desorb from the surface of the soil particle and dissolve into the aqueous phase.

Modeling MSFB dechlorination of p-chlorophenol

Multiple factors contribute to the global reaction rate including: desorption of *p*-chlorophenol from the soil particles, diffusion of the reactant to the Pd/Fe-alginate bead, boundary layer diffusion at the liquid-bead interface, adsorption at the alginate bead surface, diffusion through the alginate matrix to an active site, the intrinsic reaction rate at the Pd/Fe surface, and the rate of deactivation of the palladized iron. Sorption equilibria for both the Pd/Fe-loaded alginate beads and the Willamette Valley soil used in this study were characterized. Linear isotherms of the form $C_{bd} = K_b\, C_b$ were constructed by equilibrating 25 mL aliquots of 3.91×10^{-3} M *p*-chlorophenol with a range of alginate bead (or Willamette Valley soil) concentrations, followed by determination of the aqueous *p*-chlorophenol concentrations at equilibrium. The aqueous phase diffusion coefficient for *p*-chlorophenol was derived in a previous study.[43]

Diffusion coefficients for the fluidization media were determined by contacting alginate beads with a well mixed solution of *p*-chlorophenol at known concentration, monitoring the decline in aqueous phase concentration over time, and fitting these data to the nonsteady state diffusion model using the method of Oyaas et al.[69] Diffusion coefficients were determined for alginate beads formed over a range of gelation times between 5–60 min, corresponding to a range of bead densities. The diffusion coefficients calculated from these data are the same within experimental error in all cases ($D_e = 8 \times 10^{-10}$ m^2/s). This compares favorably with the value of 8.5×10^{-10} m^2/s reported for phenol in similarly prepared alginate media.[70]

The model developed in Eqs. 13–18 was applied to the experimental data using Euler's finite divided difference method and optimization algorithms coded in Fortran using IMSL subroutines. The minimization with simple bounds optimization procedure uses a quasi-Newton method, and a finite difference gradient to minimize the objective function

$$F = \sum (C_b(t)_{model} - C_b(t)_{expt})^2 \tag{28}$$

Using this method, values for the effective diffusion coefficient of *p*-chlorophenol in Pd/Fe media (D_e), the bulk liquid-particle mass-transfer coefficient (k_l), the reaction rate constant (k), and the deactivation rate constant (k_d) were derived. The results of

Table 3. Model Derived Parameters for MSFB Dechlorination of *p*-Chlorophenol Contaminated Soil

Parameter	Units	Model Parameters	Independently Determined Values
k_d	1/s	2.3×10^{-4}	2.3×10^{-4}
			1.33×10^{-5} Correlation (Fan *et al.,* 1960)[72]
k_l	m/s	1.3×10^{-5}	8.98×10^{-5} Correlation (Coderc *et al*., 1972)[73]
			4.37×10^{-5} Correlation (Cussler, 1984)[74]
k	m^3/s-$kg_{catalyst}$	0.021	0.021
D_e	m^2/s	8.2×10^{-10}	8.0×10^{-10} Experiment
			7.0×10^{-10} Correlation (Schwarzenbach *et al.*, 1993)[68]
			9.3×10^{-10} Correlation (Schwarzenbach *et al*., 1993)[68]
			1.1×10^{-9} Correlation (Schwarzenbach *et al*., 1993)[68]
$K_{d,s}$	(mol/kg soil)/(mol/L H_2O)	1.12	1.19 Correlation (Schwarzenbach *et al*., 1993)[68]

the modeling effort applied to MSFB dechlorination reactions for aqueous *p*-chlorophenol are illustrated in Figure 9. Values derived from the four-parameter optimization are summarized in Tables 1 and 2. Derived values for the reaction and deactivation rate constants are in good agreement with the results derived independently from batch kinetics experiments. The derived value for the effective diffusion coefficient also compares favorably with independently measured values. Clearly, the model provides a good approximation of the experimental results. Figure 9 also shows the deactivation of the palladized iron – alginate media over the course of the reaction.

The same methods were applied to the modeling of the dechlorination of *p*-chlorophenol contaminated soil (Eqs. 19–27). The results are presented in Figure 10 and Table 3. In this case, a five fold optimization was used to derive values for the soil-water sorption equilibrium constant ($K_{d,s}$) in addition to those for the other parameters. Again, the results of the modeling exercise produce a good fit to the experimental results and the values of the derived parameters agree well with those that were determined experimentally and independently.

Conclusions

Efficient chemical reactions involving viscous liquids, sludges, and other solid media are difficult to achieve because of poor contacting between the phases. Examples in industry include the remediation of liquids and sludges originating within the nuclear energy, pulp and paper, petroleum refining, and petrochemical industries. Employment of the Pd/Fe bimetallic system in the MSFB reactor provides a novel process by which to dechlorinate not only simple aqueous streams, but also viscous, particle laden, and difficult to treat streams. Iron and palladium are entrapped within polymeric beads consisting of calcium alginate. Use of this composite ferromagnetic inorganic-organic medium offers the advantage of maintaining the active beads within the bed while the slurry is fluidized. The dechlorination reaction rate is inherently fast, hence, mass transfer of the chlorinated compounds from the sludge particles to the bead surface and subsequent diffusion through the alginate polymeric matrix are limiting factors. The former limitation is overcome, since convective mass transfer is greatly enhanced within the MSFB, thereby allowing higher relative velocities between sludge and beads to be achieved than are otherwise possible in an ordinary fluidized bed.[53,54,71] To reduce the diffusion resistance, beads of smaller diameter may also be utilized. These methods can be applied to the remediation of halocarbon laden sludge systems in two ways. The first is to mobilize and extract reactants from the sludge and then treat the extracted liquid within the fluidized bed. In this process, the liquid phase is typically recycled to the extracting unit until the concentration in the sludge reaches a permissible level. The second method of treatment involves direct pumping of particle-laden streams through the MSFB. Clearly, the methods and mathematical models reported in this study for the reductive dehalogenation of *p*-chlorophenol have strong potential for application to a wide variety of additional halogenated environmental contaminants in both aqueous phase and solid matrices.

Acknowledgment

The authors acknowledge the generous support provided by the Wastemanagement Education and Research Consortium (WERC) and the U.S. Department of Energy, which made this research possible.

Notation

a = catalyst activity, dimensionless
a' = external bead surface area/unit bulk liquid volume, m^2/m^3
$\mathbf{B}$ = magnetic flux density, N/A-m
C_A = concentration of *p*-chlorophenol, mol/m^3
C_b = bulk concentration of *p*-chlorophenol in aqueous phase, mol/m^3
C_l = alginate bead liquid concentration, mol/m^3
C_{H^+} = concentration of H^+ in solution, mol/m^3
C_{H^*} = concentration of H* in solution, mol/m^3
C_s = concentration of *p*-chlorophenol on Willamette Valley type soil, mol/kg soil
D_e = diffusion coefficient for *p*-chlorophenol in alginate beads, m^2/s
ε = reactor voidage in magnetically stabilized fluidized bed, dimensionless
$\mathbf{F_m}$ = magnetic body force per unit volume, N/m^3
k_l = Liquid-solid mass transfer coefficient in MSFB, m/s
$k_{l,s}$ = mass-transfer coefficient from soil particles to bulk liquid, m/s
k = reaction-rate coefficient for *p*-chlorophenol dechlorination, $m^3/kg_{catalyst}$ s
k' = Reaction rate coefficient for *p*-chlorophenol dechlorination, $m^6/mol\text{-}kg_{catalyst}$ s
k^* = Reaction rate coefficient for *p*-chlorophenol dechlorination, m^3/s
k_d = deactivation rate coefficient for H_2 (g) passivation, 1/s
k_{ds} = mass-transfer coefficient for *p*-chlorophenol desorption from soil, 1/s
K_b = gel solid-water distribution ratio, mol/kg bead/(mol/L H_2O)
$K_{d,s}$ = Solid water distribution ratio, moles/kg soil/(moles/m^3 bulk liquid)
$\mathbf{M}$ = magnetization, A/m
n = deactivation order, dimensionless
r = bead radius, mm
t = time, s
V = volume of reactor liquid, m^3
W = weight of catalyst, g

Literature Cited

1. Benitez FJ, Beltran-Heredia J, Acero JL, Rubio FJ. Rate constants for the reactions of ozone with chlorophenols in aqueous solutions. *J. Hazard. Mater.* 2000;B79:271-285.
2. Chu W, Wong CC. A disappearance model for the prediction of trichlorophenol ozonation. *Chemosphere.* 2003;51:289-294.
3. Graham N, Chu W, Lau C. Observations of 2,4,6-trichlorophenol degradation by ozone. *Chemosphere.* 2003;51:237-243.
4. Chu W, Law CK. Treatment of trichlorophenol by catalytic oxidation process. *Water Res.* 2003;37:2339-2346.
5. Kang N, Lee DS, Yoon J. Kinetic modeling of Fenton oxidation of phenol and monochlorophenols. *Chemosphere*. 2002;47:915-924.
6. Huang HH, Lu MC, Chen JN. Catalytic decomposition of hydrogen peroxide and 2-chlorophenol with iron oxides. *Water Res.* 2001;35: 2291-2299.
7. Huang HH, Lu MC, Chen JN, Lee CT. Catalytic decomposition of hydrogen peroxide and 4-chlorophenol in the presence of modified activated carbons. *Chemosphere.* 2003;51:935-943.
8. Kasuga K, Mori K, Sugimori T, Handa M. Kinetic study on the oxidation of trichlorophenol using hydrogen peroxide and an iron(III) complex of tetrasulfonatophthalocyanine catalyst. *Bull Chem Soc Jpn.* 2000;73:939-940.
9. Hou WJ, Tsuneda S, Hirata A. TOC removal of 2,4,5-trichlorophenol synthetic wastewater with H_2O_2/UV in a batch reactor. *J Chem Eng Jpn.* 2001;34:1049-1051.
10. Fukushima M, and Tatsumi K. Degradation pathways of pentachlorophenol by photo-Fenton systems in the presence of Fe(III), humic Acid, and hydrogen peroxide. *Environ Sci Technol.* 2001;35:1771-1778.
11. Mazellier P, Bolte M. 3-Chlorophenol elimination upon excitation of dilute Fe(III) solution: evidence for the only involvement of $Fe(OH)^{2+}$." *Chemosphere*. 2001;42:361-366.

12. Nogueira RFP, Trovo AG, Mode DF. Solar photodegradation of dichloroacetic acid and 2,4-dichlorophenol using an enhanced photo-Fenton process. *Chemosphere.* 2002;48:385-391.
13. Gherardini L, Michaud PA, Panizza M, Comninellis C, Vatistas M. Electrochemical oxidation of 4-chlorophenol for wastewater treatment: eefinition of normalized current efficiency (ϕ). *J Electrochem Soc.* 2001;148:D78–D82.
14. Rodrigo MA, Michaud PA, Duo I, Panizza M, Cerisola G, Comninellis C. Oxidation of 4-chlorophenol at boron-doped diamond electrode for wastewater treatment. *J Electrochem Soc.* 2001;148:D60–D64.
15. Ureta-Zanartu MS, Bustos P, Berrios C, Diez MC, Mora ML, Gutierrez C. Electrooxidation of 2,4-dichlorophenol and other polychlorinated phenols at a glassy carbon electrode. *Electrochim. Acta*. 2002; 47:2399-2406.
16. Cheng H, Scott K, Christensen PA. Electrochemical hydrodehalogenation of chlorinated phenols in aqueous solutions. I. Material aspects. *J Electrochem Soc.* 2003;150:D17–D24.
17. Cheng H, Scott K, Christensen PA. Electrochemical hydrodehalogenation of chlorinated phenols in aqueous solutions. II. Effect of operating parameters. *J Electrochem Soc.* 2003;150:D25–D29.
18. Waldner G, Pourmodjib M, Bauer R, Neumann-Spallart M. Photoelectrocatalytic degradation of 4-Chlorophenol and oxalic acid on titanium dioxide electrodes. *Chemosphere.* 2003;50:989-998.
19. Yuan G, Keane MA. Liquid phase catalytic hydrodechlorination of chlorophenols at 273 K. *Catal Commun.* 2003;4:195-201.
20. Yuan G, Keane MA. Liquid phase catalytic hydrodechlorination of 2,4-dichlorophenol over carbon supported palladium: an evaluation of transport limitations. *Chem Eng Sci.* 2003;58:257-267.
21. Marshall WD, Kubatova A, Lagadec AJM, Miller DJ, Hawthorne SB. Zero-valent metal accelerators for the dechlorination of pentachlorophenol (PCP) in subcritical water. *Green Chem.* 2002;4:17-23.
22. Morales J, Hutcheson R, Cheng IF. Dechlorination of chlorinated phenols by catalyzed and uncatalyzed Fe(0) and Mg(0) particles. *J Hazard Mater.* 2002;B90:97-108.
23. Lee GH, Nunoura T, Matsumura Y, Yamamoto K. Effects of sodium hydroxide addition on the decomposition of 2-chlorophenol in supercritical water. *Ind Eng Chem Res.* 2002;41:5427-5431.
24. Lee GH, Nunoura T, Matsumura Y, Yamamoto K. Global kinetics of 2-chlorophenol disappearance with NaOH in supercritical water. *J Chem Eng Jpn.* 2002;35:1252-1256.
25. Yang HH, Eckert CA. Homogeneous catalysis in the oxidation of *p*-chlorophenol in supercritical water. *Ind. Eng. Chem. Res.* 1988;27: 2009-2014.
26. Agrios AG, Gray KA, Weitz E. Photocatalytic transformation of 2,4,5-trichlorophenol on TiO_2 under sub-band-gap illumination. *Langmuir.* 2003;19:1402-1409.
27. Doong RA, Chen CH, Maithreepala RA, Chang SM. The influence of pH and cadmium sulfide on the photocatalytic degradation of 2-chlorophenol in titanium dioxide suspensions. *Water Res.* 2001;35:2873-2880.
28. Lettmann C, Hildenbrand K, Kisch H, Macyk W, Maeir WF. Visible light photodegradation of 4-chlorophenol with a coke-containing titanium dioxide photocatalyst. *Appl Catal B: Environ.* 2001;32:215-227.
29. Ku Y, Hsieh CB. Photodecomposition of 2,4-dichlorophenol in aqueous solution catalyzed by cadmium sulfide particles. *Ind Eng Chem Res.* 1992;31:1823-1826.
30. Yue B, Zhou Y, Xu J, Wu Z, Zhang X, Zou Y, Jin S. Photocatalytic degradation of aqueous 4-chlorophenol by silica-immobilized polyoxometalates. *Environ Sci Technol.* 2002;36:1325-1329.
31. Ma KC, Shiu WY, Mackay D. Aqueous solubilities of chlorinated phenols at 25 °C. *J Chem Eng Data.* 1993;38:364-366.
32. Achard C, Jaoui M, Schwing M, Rogalski M. Aqueous solubilities of phenol derivatives by conductivity measurements. *J Che Eng Data.* 1996;41:504-507.
33. Balko EN, Przybylski E, Von Trentini F. Exhaustive liquid-phase catalytic hydrodehalogenation of chlorobenzenes. *Appl. Catal. B: Environ.* 1993;2:1-8.
34. Benitez JL, Del Angel G. Catalytic hydrodechlorination of chlorobenzene in liquid phase. *React. Kinet. Catal. Lett.* 1999;66:13-18.
35. Gomez-Sainero LM, Cortes A, Seoane XL, Arcoya A. Hydrodechlorination of carbon tetrachloride to chloroform in the liquid phase with metal-supported catalysts. Effect of the catalyst components. *Ind Eng Chem Res.* 2000;39:2849-2854.
36. Wang CB, Zhang WX. Synthesizing nanoscale iron particles for rapid and complete dechlorination of TCE and PCBs. *Environ Sci Technol*. 1997;31:2154-2156.
37. Lien HL, Zhang WX. Transformation of chlorinated methanes by nanoscale iron particles. *J Environ Eng*. 1999;125:1042-1047.
38. Kim YH, Carraway ER. Dechlorination of pentachlorophenol by zero valent iron and modified zero valent irons. *Environ. Sci. Technol.* 2000;34:2014-2017.
39. Liu Y, Yang F, Yue PL, Chen G. Catalytic dechlorination of chlorophenols in water by palladium/iron. *Water Res.* 2001;35:1887-1890.
40. Liu Y, Yang F, Chen J, Gao L, Chen G. Linear free energy relationships for dechlorination of aromatic chlorides by Pd/Fe. *Chemosphere.* 2003;50:1275-1279.
41. Guasp E, Wei R. Dehalogenation of trihalomethanes in drinking water on Pd-Fe^0 bimetallic surfaces. *J Chem Technol Biotechnol.* 2003;78: 654-658.
42. Zhou HY, Xu XH, Wang DH. Catalytic dechlorination of chlorobenzene in water by Pd/Fe bimetallic system. *J Environ Sci.* 2003;15:647-651.
43. Graham LJ, Jovanovic GN. Dechlorination of *p*-chlorophenol on a Pd/Fe catalyst in a magnetically stabilized fluidized bed; implications for sludge and liquid remediation. *Chem Eng Sci.* 1999;54:3085-3093.
44. Rosensweig RE. Fluidization: hydrodynamic stabilization with a magnetic field. *Science*. 1979;204:57-60.
45. Rosensweig RE. Magnetic stabilization of the state of uniform fluidization. *Ind Eng Chem Fundam.* 1979;18:260-269.
46. Rosensweig RE, Siegell JH, Lee WK, Mikus T. Magnetically stabilized fluidized solids. *AIChE Symposium Series.* 1981;77:8-16.
47. Rosensweig RE. Process concepts using field-stabilized two-phase fluidized flow. *J. Electrostatics* 1995;34:163-187.
48. Hristov JY, Magnetic field assisted fluidization - a unified approach. Part 1. Fundamentals and relevant hydrodynamics. *Rev Chem Eng.* 2002;18:295-509.
49. Hristov JY. Magnetic field assisted fluidization - a unified approach. Part 2. Solids batch gas-fluidized beds: versions and rheology. *Rev Chem Eng.* 2003;19:1-132.
50. Hristov JY. Magnetic field assisted fluidization - a unified approach. Part 3. Heat transfer - a critical re-evaluation of the results. *Rev Chem Eng.* 2003;19:229-355.
51. Graham LJ, *Dechlorination of p-chlorophenol on bimetallic Pd/Fe catalyst in a magnetically stabilized fluidized bed: experiment and theory*. Corvallis: Oregon State University; 1998. Ph.D. Thesis.
52. Jovanovic GN, Honorez L. Fluidization regimes, structure, and porosity of magnetically stabilized liquid-solid fluidized bed. AIChE Annual Meeting, paper no. 157d, November 14-18, San Francisco;1994.
53. Al-Mulhim M. *Enhancement of mass transfer coefficient in a magnetically stabilized liquid-solid fluidized bed*. Corvallis: Oregon State University; 1995. M.S. Thesis.
54. Jovanovic GN, Al-Mulhim M. Liquid-solid mass transfer in magnetically stabilized fluidized beds. AIChE Annual Meeting, paper no. 127g, November 12-17, Miami Beach, CA; 1995.
55. Atwater JE, Akse JR, Jovanovic GN, Wheeler RR, Sornchamni T. Porous cobalt spheres for high temperature gradient magnetically assisted fluidized beds. *Mater. Res. Bull.* 2003;38:395-407.
56. Burns MA, Graves DJ. Structural studies of a liquid-fluidized magnetically stabilized bed. *Chem. Eng. Commun.* 1988;67:315-330.
57. Siegell JH. Liquid-fluidized magnetically stabilized beds. *Powder Technol.* 1989;52:139-148.
58. Jovanovic GN, Sajc LM, Jovanovic ZR, Novakovic GV, Kundacovic B, Obradovic B, Vukovic DV. Flow behavior of fluidized beds in a magnetic field. *J Serb Chem Soc.* 1992;57:345-352.
59. Fee CJ. Stability of the liquid-fluidized magnetically stabilized fluidized bed. *AIChE J*. 1996;42:1213-1219.
60. Burns MA, Graves DJ. Continuous affinity chromatography using a magnetically stabilized fluidized bed. *Biotechnol Prog.* 1985;1:95-103.
61. Goetz V, Graves DJ. Axial dispersion in magnetically stabilized fluidized bed liquid chromatography column. *Powder Technol.* 1991;64: 81-92.
62. Zhang Z, O'Sullivan DA, Lyddiatt D. Magnetically stabilized fluidized bed adsorption: practical benefit of uncoupling bed expansion from fluid velocities in the purification of a recombinant protein from *Escherichia coli*. *J Chem Technol Biotechnol*. 1999;74:270-274.
63. Ames TT, Worden RM. Continuous production of daidzein and genistein from soybean in a magnetofluidized bed bioreactor. *Biotechnol Prog.* 1997;13:336-339.

64. Bohm D, Pittermann B. Magnetically stabilized fluidized beds in biochemical engineering - investigations in hydrodynamics. *Chem Eng Technol.* 2000;23:309-312.
65. Graham LJ, Jovanovic GN. Catalytic dechlorination of chlorinated hydrocarbons in magnetically stabilized bluidized Bed (MSFB*). World Congress on Particle Technology*, July 7-9, Brighton, UK; 1998.
66. Matheson LJ, Tratnyek PG. Reductive dehalogenation of chlorinated methanes by iron. *Envrion Sci Technol.* 1994;28:2045.
67. Plonski IH. Kinetics of active iron dissolution inhibited by adsorbed hydrogen. *Int J Hydrogen Energy*. 1997;22:1005-1020.
68. Schwarzenbach RP, Gschwend PM, Imboden DM. *Environmental Organic Chemistry*. New York: Wiley;1993.
69. Oyaas J, Storre I., Lysberg M, Svendsen H, Levine DW. Determination of effective diffusion coefficients and distribution constants in polysaccharide gels with non-steady-state measurements. *Biotechnol Bioeng*. 1995;47:501-507.
70. Shishido M, Kojima T, Araike YK, Toda M. Biological phenol degradation by immobilized activated sludge in gel bead with three phase fluidized bed bioreactor. *Trans Inst. Chem Engr*. 1995;73: 719-726.
71. Rhee BK. *Enhancement of mass transfer coefficient in a three-phase magnetically stabilized fluizied bed*. Corvallis: Oregon State University, Corvallis; 1998. M.S. Thesis
72. Fan L. Fluidization as an Undergraduate Unit-Operation Experiment. *J Chem Ed.* 1960;37:259.
73. Couderc JP, Gibert H, Angelino H. Transfert de materiere par diffusion en fluidisation liquide. *Chem. Eng. Sci.* 1972;27:11-20.
74. Cussler EL. *Diffusion: Mass Transfer in Fluid Systems*. New York: Cambridge University Press; 1984.

Manuscript received Aug. 15, 2004, and revision received Aug. 4, 2005.